

This work was written as part of one of the author's official duties as an Employee of the United States Government and is therefore a work of the United States Government. In accordance with 17 U.S.C. 105, no copyright protection is available for such works under U.S. Law.

Public Domain Mark 1.0

<https://creativecommons.org/publicdomain/mark/1.0/>

Access to this work was provided by the University of Maryland, Baltimore County (UMBC) ScholarWorks@UMBC digital repository on the Maryland Shared Open Access (MD-SOAR) platform.

Please provide feedback

Please support the ScholarWorks@UMBC repository by emailing scholarworks-group@umbc.edu and telling us what having access to this work means to you and why it's important to you. Thank you.

Dipolarization and turbulence in the plasma sheet during a substorm: THEMIS observations and global MHD simulations

Mostafa El-Alaoui,^{1,2} Robert L. Richard,^{1,2} Maha Ashour-Abdalla,^{1,2} Melvyn L. Goldstein,³ and Raymond J. Walker^{4,5}

Received 14 August 2013; revised 20 November 2013; accepted 23 November 2013; published 27 December 2013.

[1] Spacecraft in the magnetotail have observed fluctuations in velocity and magnetic field that have the characteristics of fluid turbulence. We investigated the properties of these fluctuations during a substorm on 7 February 2009. During this event several spacecraft were observing the magnetotail. By using upstream observations performed by Wind, we conducted a global magnetohydrodynamic (MHD) simulation of the substorm. The simulation results were compared to time series of Time History of Events and Macroscale Interactions during Substorms (THEMIS) observations in the magnetotail, and it performed well as the spacecraft encountered dipolarizations and strong flows. Further, the power spectral densities and probability distribution functions observed in the magnetotail by THEMIS and in the MHD simulations were similar. Notable features of the event include a large dipolarization growing by accreting smaller earthward moving dipolarization fronts. The dipolarizations were associated with a strong channel of earthward flow and a large vortex. In the MHD simulation results, which are supported by the observations, strong narrow flow channels are a clear and persistent feature of magnetotail convection which exist at the driving scales for the turbulent spectra.

Citation: El-Alaoui, M., R. L. Richard, M. Ashour-Abdalla, M. L. Goldstein, and R. J. Walker (2013), Dipolarization and turbulence in the plasma sheet during a substorm: THEMIS observations and global MHD simulations, *J. Geophys. Res. Space Physics*, 118, 7752–7761, doi:10.1002/2013JA019322.

1. Introduction

[2] There is considerable observational evidence of the presence of turbulence in the plasma sheet [Montgomery, 1987; Borovsky *et al.*, 1997; Lui, 2001; Borovsky and Funsten, 2003; Weygand *et al.*, 2005, 2006, 2007]. Antonova [1985] and Antonova and Ovchinnikov [1999] concluded that the fluctuations were capable of producing intense mixing in the plasma sheet. Borovsky *et al.* [1997] and Borovsky and Funsten [2003] examined fluctuations of the magnetic field and flow velocity in the plasma sheet. They concluded that the power law indices of the fluctuations' power spectral densities (PSDs) ranged between -0.8 to -2.0 for the flow and -1.6 to -3.0 for the magnetic field. Weygand *et al.* [2005] comment that these ranges

include both the theoretical value for the spectral index of $-5/3$ predicted by Kolmogorov [1941] for a neutral fluid and the $-3/2$ spectral index calculated by Kraichnan [1965] for ideal incompressible MHD turbulence. Weygand *et al.* [2005] calculated quite a broad range of magnetic field spectral indices, averaging -2.0 . A spectral index of -1.56 was found for the component of the magnetic field perpendicular to both the main field and the radial direction. Based on the scaling behavior of the probability distribution functions and the multifractal structure function, Weygand *et al.* [2005] suggested the presence of intermittent turbulence. Borovsky and Funsten [2003] proposed that the wide range of observed spectral indices might be caused by boundary fluctuations or a combination of drivers.

[3] Magnetic reconnection has been identified as the major driver of large-scale magnetotail flows during substorms [Ashour-Abdalla *et al.*, 1999, 2002; El-Alaoui *et al.*, 2009, 2010]. Ohtani *et al.* [2009] examined in detail the tailward flow measured by Geotail in a narrow region of the central plasma sheet. They found that 37% of the magnetic flux transport toward the Earth is negated by tailward transport in return flows. This ratio is larger than that observed farther down the tail. This is contrary to what one expects in a simple convection model. Ohtani *et al.* [2009] suggested that the rebound of fast earthward flows is a likely cause of high-speed tailward flows whose tailward flow velocity occasionally exceeds 200 km/s. Keiling *et al.* [2009] found that four clustered Time History of Events and Macroscale Interactions during Substorms (THEMIS) spacecraft were within one

¹Institute of Geophysics and Planetary Physics, University of California, Los Angeles, California, USA.

²Department of Physics and Astronomy, University of California, Los Angeles, California, USA.

³Heliospheric Physics Laboratory, Goddard Space Flight Center, Greenbelt, Maryland, USA.

⁴Department of Earth and Space Sciences, University of California, Los Angeles, California, USA.

⁵Now at the National Science Foundation, Arlington, Virginia, USA.

Corresponding author: M. El-Alaoui, Institute of Geophysics and Planetary Physics, University of California, 405 Hilgard Ave., Los Angeles, CA 90095, USA. (mostafa@igpp.ucla.edu)

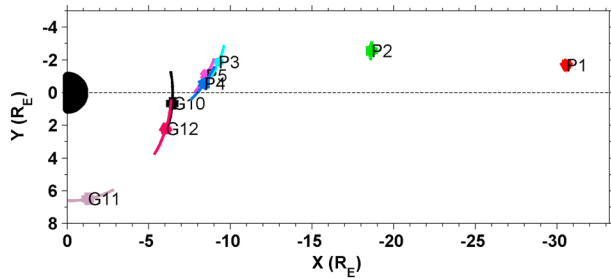


Figure 1. Projection of spacecraft trajectories onto the equatorial plane between 0300 and 0500 UT (marked points are at 0400 UT).

plasma flow vortex during a substorm, while the fifth spacecraft was in an oppositely directed flow vortex. At the same time, ground measurements indicated equivalent ionospheric currents featuring a pair of oppositely rotating flow vortices. Keiling *et al.* [2009] concluded that the magnetospheric vortices were driving the ionospheric vortices.

[4] The statistical properties of fluctuations observed by spacecraft seem to support the presence of turbulence in the magnetotail in the (low) frequency range described by MHD [Montgomery, 1987]. Global MHD simulations driven by constant or simplified solar wind/interplanetary magnetic field (IMF) conditions produce magnetotail fluctuations with spectral properties similar to observations [El-Alaoui *et al.*, 2010, 2011, 2012]. El-Alaoui *et al.* [2010, 2012] found PSDs and probability distribution functions (PDFs) that are consistent with in situ observations and with theory. Localized reconnection was identified as the main process driving turbulence.

[5] In a global magnetohydrodynamic (MHD) simulation, El-Alaoui *et al.* [2009] found near-Earth flow vortices that agreed with magnetospheric observations taken at THEMIS P3 and P4. Around the time of substorm onset, flow vortices formed in the simulation near the locations of the two spacecraft. Although the simulated flows appeared to be turbulent, the high time resolution output necessary to confirm the turbulent fluctuation spectra had not been acquired. To verify that the flows in the magnetotail are actually turbulent, we extended the study by El-Alaoui *et al.*, [2010, 2012] by performing an event simulation driven by upstream solar wind observations with both high temporal and spatial resolution. The results, reported in this paper, strongly suggest that the plasma sheet was turbulent. The simulation reproduced not only the overall magnetotail changes observed by spacecraft but also the spectral properties of the turbulence the spacecraft observed.

2. Flow Vortices and Dipolarization in the Plasma Sheet

[6] We chose the 7 February 2009 substorm event to simulate the plasma sheet and its spectrum of fluctuations. During this substorm, the *AE* index reached approximately 125 nT. Eight spacecraft were located in different regions of the magnetosphere during the time of interest (0300 UT to 0500 UT). These included the five THEMIS spacecraft, which were all on the dawnside of the magnetotail. The geosynchronous spacecraft GOES-10, GOES-11, and GOES-12 were near 0, 19, and 23 h magnetic local time, respectively. In Figure 1 the locations of the eight spacecraft are projected onto the noon-midnight

meridian plane (GSM coordinates). THEMIS P4 (E), P5 (A), and P3 (D) were located close to each other at $8.4 R_E$, $8.5 R_E$, and $9.4 R_E$ down tail, respectively. The location of THEMIS P2 (C) was at $x = -18.6 R_E$, and the location of THEMIS P1 (B) was $x = -30.6 R_E$.

[7] Lyons *et al.* [2012] determined substorm onset to be at 0347:12 UT near the longitude of GOES-10. Activity propagated to the locations of GOES-12, P4, P3, and P5 during the expansion phase. From THEMIS all-sky cameras, Lyons *et al.* [2012] identified three streamers extending toward the equator starting at ~ 0357 UT. The first was near the longitude of GOES-12, and the others were near the longitudes of P3, P4, and P5. They noted that significant dipolarization was associated with the streamers after 0400 UT rather than at onset. GOES-10 did not observe a dipolarization until about 25 min after onset although it was close to the initial onset in longitude [Lyons *et al.*, 2012]. Oka *et al.* [2011] showed that increased field line stretching seen at P3, P4, and P5 in the inner magnetosphere was associated with a tailward retreat of the *X*-line detected by P1 located near $-30 R_E$. P2 was in an intermediate position and observed increasing total pressure at this time. They concluded that the pressure increase eventually caused the *X*-line to move tailward.

[8] During the time of interest (0300–0500 UT) the Wind spacecraft was located on the dawnside ($y = -73 R_E$) $202.0 R_E$ sunward of Earth at $z = -38 R_E$ (GSM coordinates). Wind observations were used to drive our global MHD simulation [Raeder *et al.*, 1995]. Figure 2 shows time series of IMF and solar wind plasma on the upstream boundary of the simulation at $x = 25 R_E$. These have been shifted uniformly by 55 min

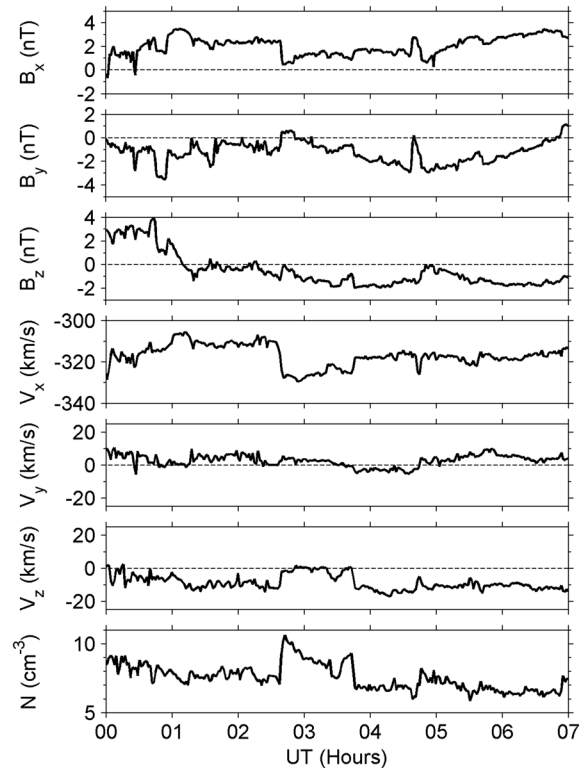


Figure 2. Solar wind data on 7 February 2009 from Wind. (top to bottom) The components of the magnetic field, velocity, and proton density.

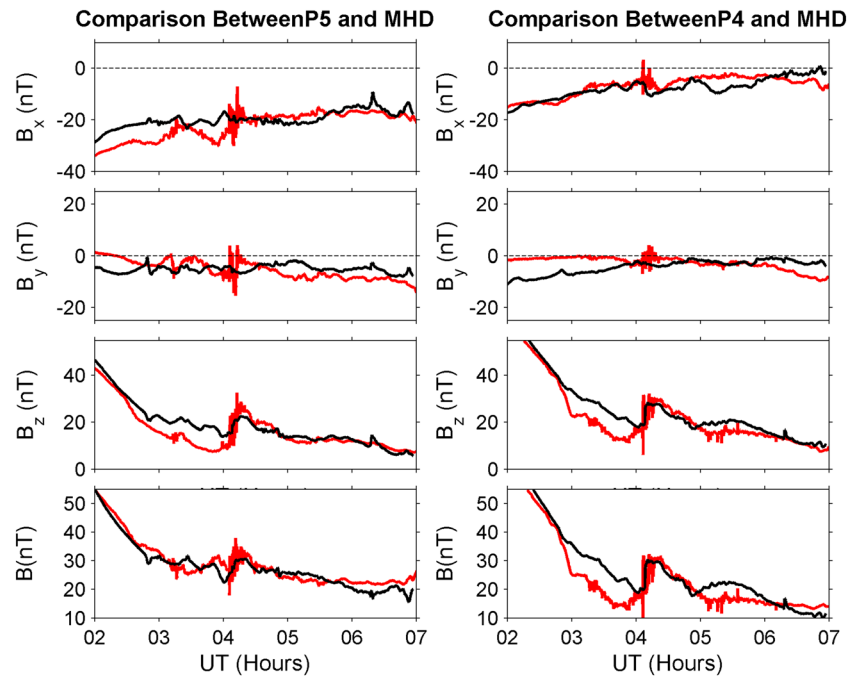


Figure 3. A comparison of observed magnetic field time series from (left) THEMIS P5 and (right) THEMIS P4 with simulation results. The data are shown in red and the MHD simulation results in black.

from the Wind observations because of the time it takes for the solar wind to move from Wind to the boundary of the MHD simulation. This includes the time varying B_x component, which requires special consideration, as discussed in *El-Alaoui* [2001]. In order to conserve the divergence of the magnetic field, we therefore determine a minimum variance coordinate system for the driving upstream IMF and then set the IMF component along the minimum variance direction to a constant value. The resulting magnetic field time series is then rotated back to GSM coordinate for use as input to the simulation. The IMF B_x component was directed sunward. The IMF B_y was variable but mostly downward directed. The time history of the IMF B_z before and during the interval of interest can be divided into

three intervals: prior to 0109 UT it was northward, from 0109 to 0242 UT it fluctuated narrowly around zero, and then at 0242 UT it turned southward and remained southward until after 0500 UT. It is likely that the third interval of southward IMF drove the substorm event that started at 0347 UT. During this interval the solar wind density increased slightly. The solar wind speed was 320 km/s, and the magnitudes of V_y and V_z remained less than 20 km/s.

[9] MHD output and THEMIS P4 magnetic field measurements from 0200 UT to 0700 UT are compared in Figure 3 (right). The passage of a strong dipolarization front near 0400 UT is prominent in both the observations and the simulation. The magnetic field observations at 3 s intervals are

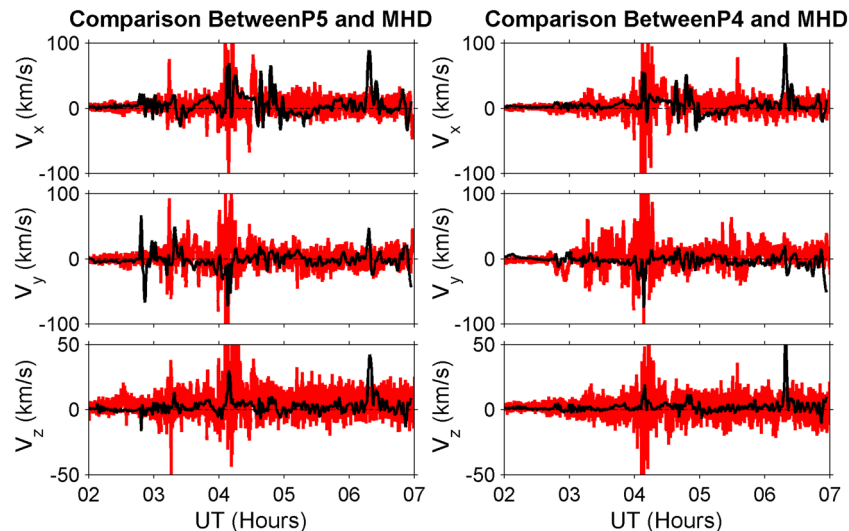


Figure 4. A comparison of observed flow velocity components from (left) THEMIS P5 and (right) THEMIS P4 with simulation results. The data are shown in red and the MHD simulation results in black.

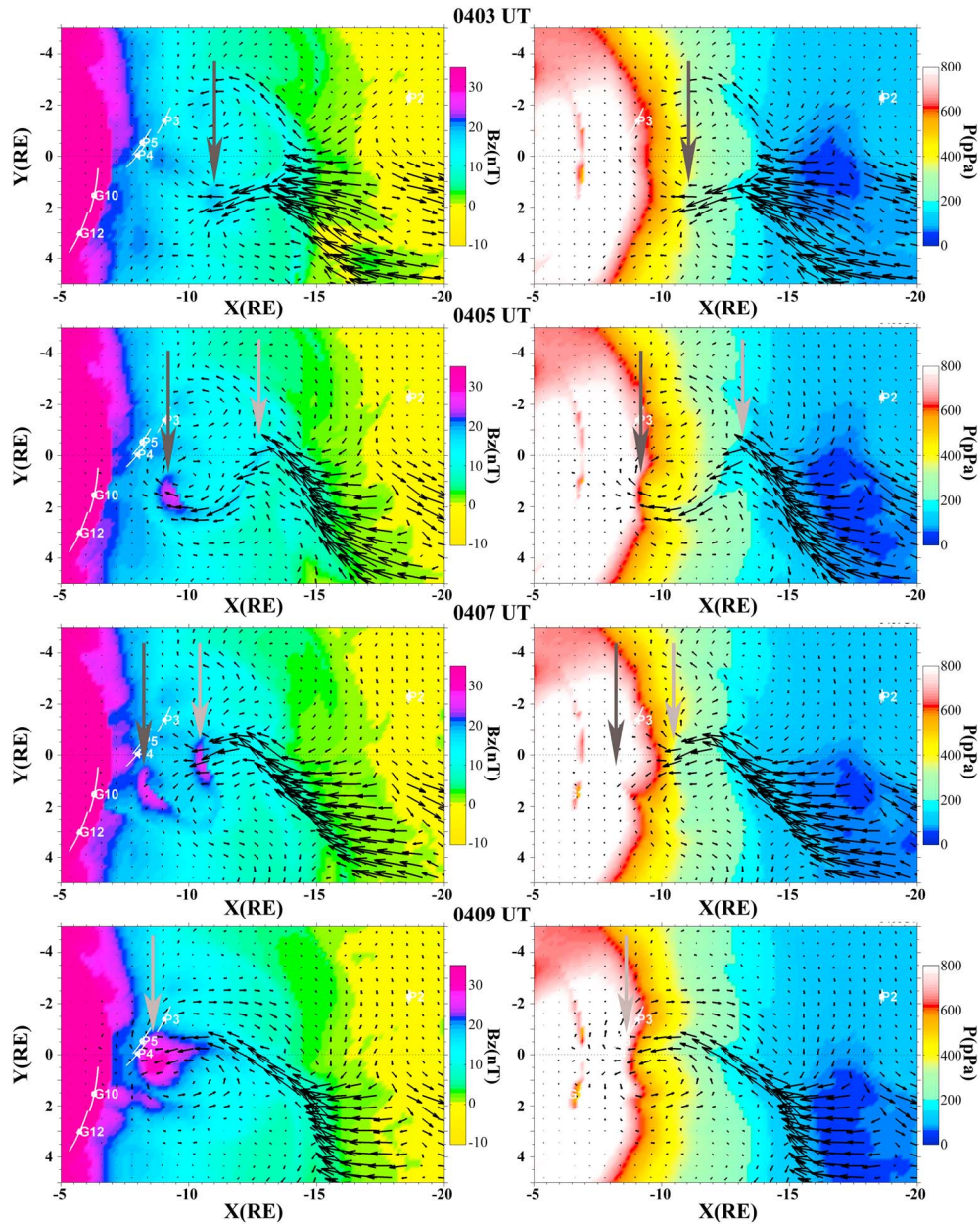


Figure 5. MHD results in the maximum pressure surface are shown at four times. (right) Color contours show the z component of the magnetic field (plasma pressure), and the black arrows give the flow velocity on the maximum pressure surface. The white segments in each plot indicate the positions of spacecraft projected onto the maximum pressure surface. Two dipolarization fronts are indicated by large vertical arrows. Dipolarization fronts are clearly visible as earthward propagating areas of high magnetic field. GSM coordinates are used.

indicated in red. The black lines indicate MHD results obtained at 20 s intervals. Around 0400 UT, THEMIS P4 was within the dipolarized region as indicated by the time history of B_z . THEMIS P4 measured a value of B_x indicating that the spacecraft was located in the southern plasma sheet and was never close to the center of the current sheet. Important features in the observations also occur in the simulation. In particular, the timing and magnitude of the dipolarization front apparent in the B_z component was quite similar in the observations and in the simulation. The period of enhanced B_z was greater than 30 min. Higher-frequency fluctuations do not have a one to one correspondence

between the simulation and the observations, but as we will show, their statistical properties are similar. THEMIS P5 saw developments similar to THEMIS P4 (Figure 3, left). The magnetic field's y component was relatively small and had an overall slow drift at both spacecraft that was reproduced by the simulation at both P4 and P5, with a better match at P4.

[10] Figure 4 shows the velocity components V_x , V_y , and V_z taken every 3 s from the plasma instruments (ESA) on P5 (left) and on P4 (right), versus time, as well as MHD simulation results taken every 20 s. The MHD model results are in general agreement with observations in that intervals

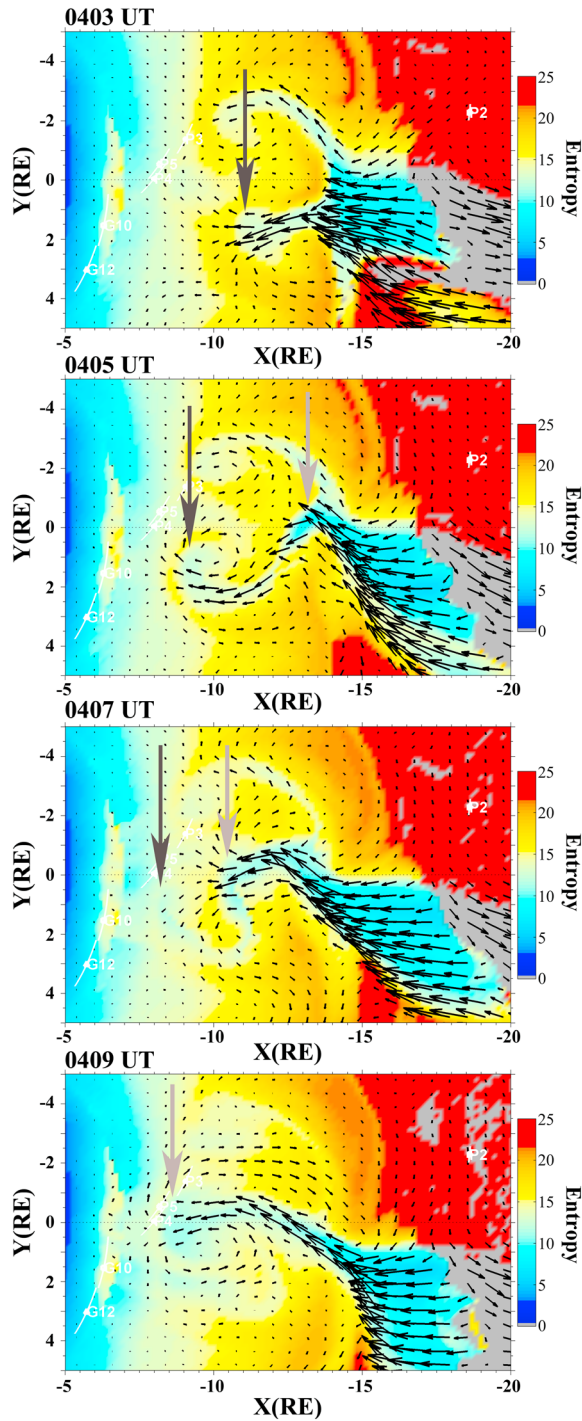


Figure 6. For the same region as shown in Figure 5, the entropy is indicated by color contours. The black arrows give the flow velocity on the maximum pressure surface. The white segments in each plot indicate the positions of spacecraft projected onto the maximum pressure surface. Two dipolarization fronts are indicated by large vertical arrows as in Figure 5. Gray areas correspond to IMF field line regions where the entropy is not calculated.

of strong, variable flows often coincide. In particular, simulation and observations in the interval around 0400 UT, near the arrival time of the dipolarization front, include enhanced downward and duskward flows.

[11] We have shown that the MHD simulation includes the major changes during the substorm event as observed by THEMIS P5. The geosynchronous spacecraft observations (GOES 11 and 12) show only slow variations in the magnetic field (not shown) which are captured by the simulation. THEMIS P3, downward of P5, observed the same dipolarization seen by P4 and P5, but the MHD simulation overpredicted the strength of a small prior dipolarization. P1 and P2 observations show large fluctuations consistent with proximity to an active reconnection region. The simulation shows a similar pattern of large fluctuations there though the detailed sequence is different. In particular, the observed fluctuations at high frequencies are larger in the observations. When we solve the MHD equations, dissipation effectively smooths the time series. For this paper we will concentrate on the well-reproduced dipolarization seen by P4 and P5. When the spacecraft are placed in the context of the overall magnetotail seen in the MHD simulation, the observations by the various spacecraft form a coherent picture. Simulation results in the vicinity of THEMIS P3, P4, and P5 before and during the dipolarization are displayed in Figure 5. These results are at the surface of maximum pressure [Ashour-Abdalla *et al.*, 2002; Perroomian *et al.*, 2006; El-Alaoui *et al.*, 2009], a proxy for the current sheet, and are projected into the equatorial plane. The snapshots on the left show the B_z component of the magnetic field and the flow velocity vectors on the maximum pressure surface (x and y) at four key times between 0403 UT and 0411 UT.

[12] Even though the vector parameters are displayed on a nonplanar surface, they are shown in GSM coordinates. The positions of THEMIS P3, P4, P5, and P2 as well as GOES 10 and 12 are also projected onto the surface. Several dipolarization fronts were seen in the simulation. These earthward moving dipolarization fronts can be seen in this format as localized increases in the B_z component (purple regions). The dipolarization fronts are at the earthward ends of channels of strong flow. At 0407 UT there were at least two clear dipolarization fronts apparent around $-8 R_E$ and $-12 R_E$. These dipolarization fronts and associated narrow channels of earthward flow started near a neutral line further down tail. The flows in these channels, combined with lower velocity return flows, form several vortices in the plasma sheet. The first dipolarization occurred on the duskside and missed the THEMIS spacecraft locations. The second dipolarization occurred around midnight and was observed by the P3, P4, and P5 spacecraft. Figure 5 (right) shows the thermal pressure and flows in the same format. The flow channels exhibit lower pressure and higher B_z than adjacent regions; in particular, the pressure behind the front decreases by about factor of 2.

[13] Figure 6 shows the entropy and components of the flow velocity. In this calculation the entropy is calculated by using the following equation [Birn *et al.*, 2004, 2011]:

$$S = \int P^{1/\gamma} \frac{ds}{B}$$

[14] In this equation the integral is taken along a closed field line from the northern to the southern ionosphere; P represents the plasma pressure, and B is the magnitude of the magnetic field. The entropy in the dipolarization region and

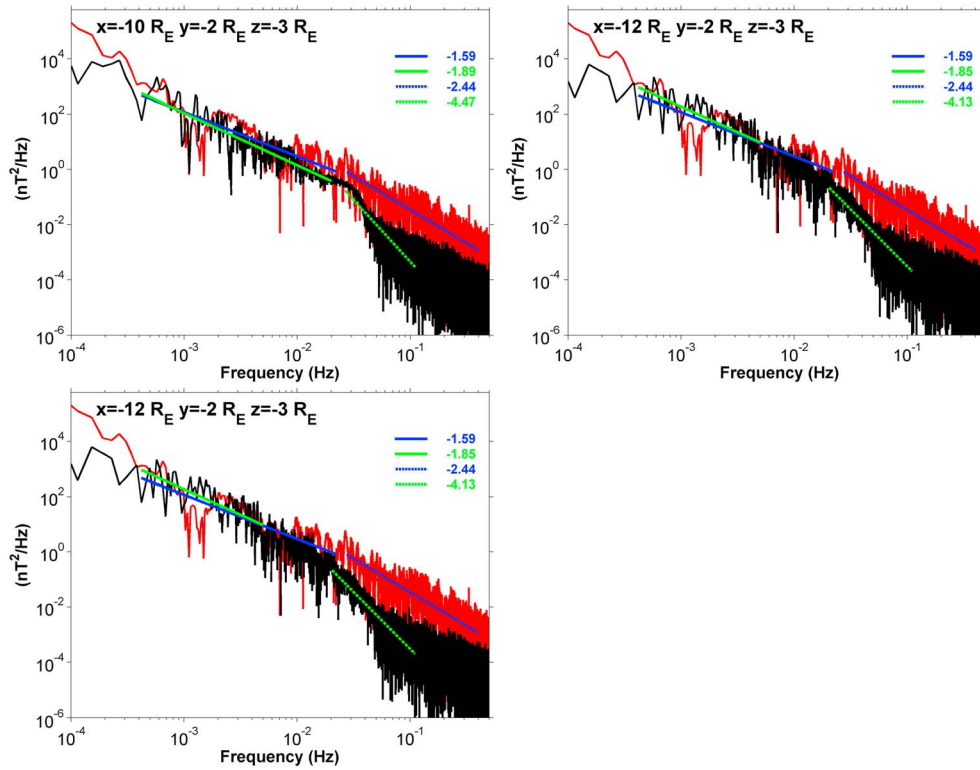


Figure 7. The panels show PSDs for B_z at the three locations in the MHD simulation listed in the panels (black) and at THEMIS P5 (red). The solid blue (green) lines are least squares fits in the inertial range for THEMIS data (MHD results). The dashed blue (green) lines are least squares fits in the dissipative range for THEMIS data (MHD results).

the narrow channels was low compared to the surrounding regions similar to what was found by *Birn et al.* [2004, 2011].

[15] Theoretical analysis [*Kolmogorov*, 1941] indicates that there are three frequency ranges in a turbulent fluid: a driving (energy-containing) scale at the largest scales, an inertial range at intermediate scales, and a dissipative scale at the shortest scales. Observations may not capture all three ranges, in particular the dissipative range [e.g., *Bruno and Carbone*, 2005; *Alexandrova et al.*, 2013]. Power law distributions in the PSDs are expected in the inertial and in the dissipative scale. A steeper slope is expected in the dissipative range. We tested the realism of the simulated turbulent spectra by comparing the PSDs calculated from observations at P5 with those at nearby locations in the simulation. PSDs of the north-south (z) component of the magnetic field were calculated from the simulation by using times between 0200 UT and 0500 UT, at $z = -3$ and $y = -2 R_E$ for three x values: $-10 R_E$, $-12 R_E$, and $-14 R_E$. The results are shown in Figure 7. The driving, inertial, and dissipative scales appear in both the observations and the simulation. A flat part of the spectrum in the MHD results appears at high frequencies as the MHD time step size (typically between 0.01 and 0.1 s) is approached. The spectra show changes in slope at transitions from one range to the next. At all three locations, the transitions occur at similar frequencies. The PSD slopes in the inertial and dissipative ranges were calculated by using least squares fits.

[16] The PSDs calculated from P5 measurements and from the simulations (Figure 7) exhibited power levels in the driving and inertial ranges that were close enough for the traces to

frequently overlap. Around the dissipative range there is more power in the observations, consistent with Figure 4, which showed greater fluctuations at high frequency in the observations. This is likely to be the result of dissipation and finite grid resolution in the MHD simulation with the additional possibility of kinetic processes that are not included in MHD affecting the observations. The spectral indices in the inertial range are similar, with an observed index at P5 of -1.6 and indices in the simulation ranging from -1.85 to -1.89 . In the dissipative range the PSD slope is steeper in the simulation than in the observations, though the breakpoints between the inertial and dissipative ranges both appear to be close to 25 mHz. The slope in the dissipative range from THEMIS is comparable to the result in *Vörös et al.* [2004], which is calculated from Cluster observations. We also show fits to the PSDs in the dissipative range and the resulting slopes.

3. Probability Distribution Functions

[17] Another way to characterize fluctuations is to compute probability distribution functions (PDFs). This method has been applied by *Weygand et al.* [2005, 2006] to fluctuations in the magnetic field observed by Cluster during several plasma sheet crossings. A decrease in the kurtosis, a measure of the non-Gaussian wings in the PDF, with increasing lag τ has been identified as a signature of intermittent turbulence [*Anselmet et al.*, 1984; *Castaing et al.*, 1990; *Sorriso-Valvo et al.*, 1999; *Wan et al.*, 2012; *Greco et al.*, 2012; *Osman et al.*, 2012]. Intermittent turbulence features a concentration

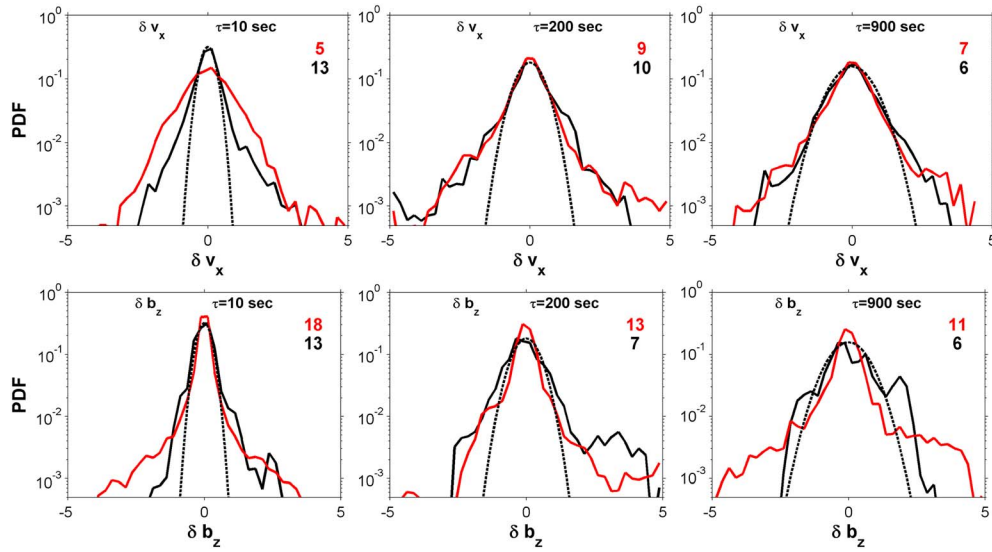


Figure 8. Probability distribution functions (PDFs) from MHD in black and for the THEMIS observations in red. (top row) From the V_x component of the flows. (bottom row) From the B_z component of the magnetic field. The kurtosis associated with each PDF is shown in red (black) for the observations (simulations).

of dissipation in a localized region. In the magnetosphere, Weygand *et al.* [2005] found that the observed PDFs are non-Gaussian for small time separations and that the kurtosis decreases for increasing time and space point separations. They attributed this decrease to the presence of intermittent turbulence.

[18] We calculated PDFs from the simulation and from THEMIS observations by using the same method as Weygand *et al.* [2005], which has also been used to analyze MHD simulation results [El-Alaoui *et al.*, 2010]. As discussed by Weygand *et al.* [2005], the values of a time lag parameter τ included in the

PDF calculation correspond to spatial lengths determined by the plasma speed. Figure 8 (top row) shows PDFs for the x component of the flow velocity from the simulation (black) and from THEMIS P5 observations (red). PDFs for a component of the magnetic field (B_z) from the simulation (black) and the THEMIS P5 observations (red) are shown in Figure 8 (bottom row). The calculations were carried out for three different values of τ . The sampling interval of the magnetic field is 0.5 s in the simulation and 0.25 s in the observations, and the sampling interval of the plasma moments is 3 s. The PDFs were taken

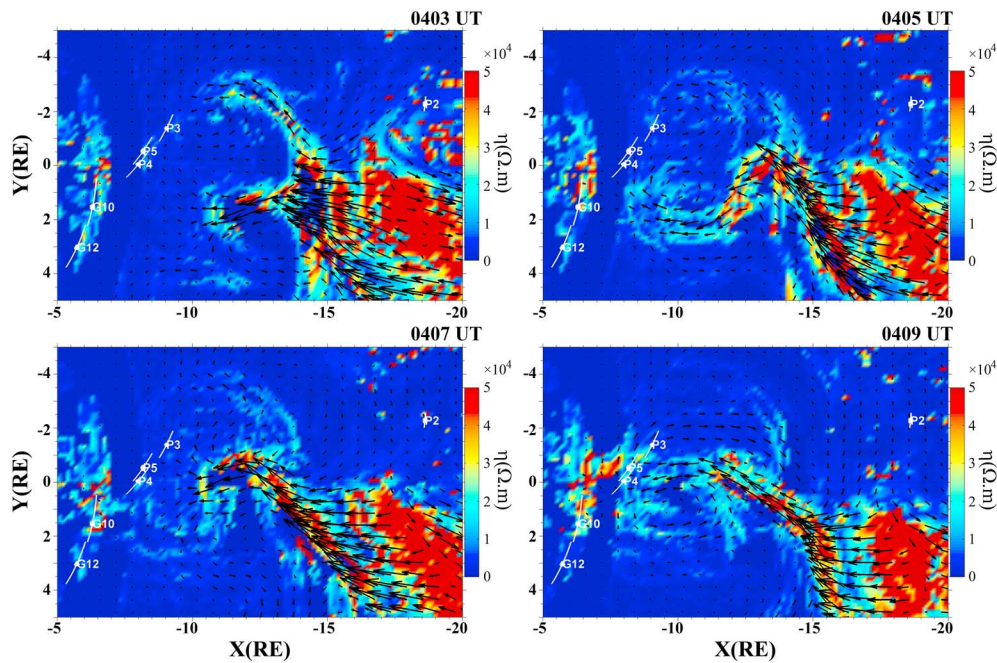


Figure 9. Localization of dissipation. For four times, which are the same as in Figure 5, color contours show the resistivity in the simulation and black arrows display the flow velocity on the maximum pressure surface.

at $x = -10 R_E$, $y = -2 R_E$, and $z = -3 R_E$. We fit Gaussian distributions by eye to the central parts of the PDFs in the simulation. If the fluctuations were random, the result would be a Gaussian distribution. Instead, all the PDFs depart from this distribution. This is manifested as features reminiscent of “wings”. The PDFs are the most similar to Gaussian distributions for $\tau = 900$ s. The similarity between the simulation and the observations is striking. The PDFs calculated in Weygand *et al.* [2005] used the same values of τ as in Figure 8. We chose different parameters (B_z and V_x) to analyze because we had a smaller number of data points (shorter time interval) closer to the current sheet. Nevertheless, the PDF shapes are similar. The kurtosis associated with the PDF of a time series should decrease with increasing time lag τ for intermittent turbulence. A kurtosis of 3 corresponds to random (Gaussian) fluctuations, while a value greater than 3 indicates excess energy at the larger (driving) scales, reflected in the wings at large deviations [Weygand *et al.*, 2005]. As can be seen in Figure 8, all the PDFs for both data and observations follow this trend except for the V_x PDF that uses a time lag of 10 s. This analysis largely supports intermittent turbulence.

4. Conclusions

[19] The simulation results showed changes similar to those seen in the observed magnetic field and plasma flow during the event. The MHD simulation results show that the evolution of the magnetosphere during this substorm was complex. In particular, dipolarizations are seen at the earthward ends of fast flow channels associated with localized reconnection. Observations have shown reconnection regions that extend only partway across the tail [e.g., Yermolaev *et al.*, 1999; Sergeev *et al.*, 1995, 1996]. Localized reconnection is also encountered in theoretical analyses [Chang, 1999] and global MHD substorm simulations [e.g., Ashour-Abdalla *et al.*, 1999]. This paper also features localized reconnection as the major cause of changes in the magnetotail.

[20] Further, we found that PSDs and PDFs computed from the simulation had the properties of fluid turbulence and that they were comparable to those seen in observations at THEMIS P5. Nested vortices on multiple scales were seen in the simulation. The largest scales were associated with reconnection outflows that were diverted in the near-Earth region.

[21] The PSD slopes from the observations and the simulations both steepen, as shown in Figure 7, at about 25 mHz. This is a feature we expect where the inertial range ends and the dissipative range begins. This further supports the idea that the simulation correctly represents the amount of dissipation at higher frequencies. The overall level of dissipation controls the location of this break point. The agreement between the break points in the simulation and the observations indicates that the level of dissipation in the simulation is realistic, even though the PSD slopes are different in the dissipative range. The resistivity model [Raeder *et al.*, 1996] sets a minimum current density at which resistivity is activated. When the magnetotail current sheet thins, the current density increases until the threshold for resistivity is reached; then resistive dissipation tends to prevent further thinning. Thus, the resistivity threshold imposes a physical scale size for the current sheet even though ideal MHD does

not include a characteristic scale. A further property of resistivity in the simulation is its localization as illustrated in Figure 9, which shows that the enhanced dissipation regions are around reconnection regions and flow channels. In this paper, as in El-Alaoui *et al.* [2012], we find the breakpoints in the PSD slopes to occur at a consistent level, even though the resistivity is localized, suggesting that the turbulent fluctuations' energy is being transported efficiently to the locations of high dissipation. As a result, the scale length of the transition to the dissipative regime is controlled by the maximum, as opposed to local, resistive dissipation. This result could help explain the low value of the magnetotail Reynolds number calculated by Weygand *et al.* [2007]. Regions of high resistive dissipation in Figure 9 are associated with strong flow channels and large flow vortices as well as thin current sheets.

[22] The magnitude of the resistivity and ionospheric dissipation also undoubtedly influence the dissipative scale length. The resistivity model has been adjusted based on previous experience with multiple-event studies [Frank *et al.*, 1995; Raeder *et al.*, 1998, 2001; Ashour-Abdalla *et al.*, 1999, 2000, 2002; El-Alaoui, 2001; El-Alaoui *et al.*, 2004, 2008, 2009; Walker *et al.*, 2006]. The simulation results in these studies showed general agreement with the spacecraft observations. Dissipation in the form of resistivity is necessary for the magnetic reconnection that drives dipolarization and magnetospheric convection as a whole in addition to providing dissipation. Mechanisms that dissipate energy at the high-frequency end of the inertial scale are necessary for the development of a turbulent cascade. Intermittent turbulence is indicated by the non-Gaussian PDFs at the upper frequencies of the inertial range. The intermittent turbulence indicated by our PDFs suggest localization of dissipation [Biskamp, 1993], which is consistent with the fact that the resistivity model in the simulation is limited in extent by the dependence on current density.

[23] High-speed outflows and localized reconnection in this simulation further support its importance in driving the turbulent cascade [El-Alaoui *et al.*, 2010, 2012]. The diversion of high-speed flows near the Earth drives the largest-scale vortices. It is possible that the intense spectrum of turbulent vortices feeds back on the reconnection process. A major factor preventing this from being a definitive conclusion is that both event studies and idealized simulations always feature flow channels, and thus, we lack a clear “control” case. Nevertheless, we have demonstrated that simulations are a useful tool in understanding magnetotail processes over a wide range of scales.

[24] **Acknowledgments.** This research was supported by NASA grants NNX10AQ47G and NNX08AO48G to UCLA. It was further supported by a grant to the Goddard Space Flight Center by the Magnetospheric Multiscale project Interdisciplinary Scientist program. R.J. Walker's contribution was made as part of his Individual Research and Development while he was at the National Science Foundation. We acknowledge NASA contracts NAS5-02099 and V. Angelopoulos for use of data from the THEMIS Mission. We further acknowledge C.W. Carlson and J.P. McFadden (ESA data), and K.H. Glassmeier, U. Auster, and W. Baumjohann (FGM data) for THEMIS observations. The MHD computations were performed by using the Gordon supercomputer at San Diego, part of the Extreme Science and Engineering Discovery Environment (XSEDE). This program is supported by grant OCI-1053575 from the National Science Foundation.

[25] Masaki Fujimoto thanks the reviewers for their assistance in evaluating this paper.

References

- Alexandrova, O., C. H. K. Chen, L. Sorriso-Valvo, T. S. Horbury, and S. D. Bale (2013), Solar wind turbulence and the role of ion instabilities, [astro-ph.SR].
- Anselmet, F., Y. Gagne, E. J. Hopfinger, and R. A. Antonia (1984), Higher-order velocity structure functions in turbulent shear flows, *J. Fluid Mech.*, **140**, 63–89.
- Antonova, E. E. (1985), Nonadiabatic diffusion and equalization of concentration and temperature in the plasma layer of the magnetosphere of the Earth, *Geomagn. Aeron.*, **25**, 517–520 (Engl. Trans.).
- Antonova, E. E., and I. L. Ovchinnikov (1999), Magnetostatically equilibrated plasma sheet with developed medium-scale turbulence: Structure and implications for substorm dynamics, *J. Geophys. Res.*, **104**(A8), 17,289–17,297, doi:10.1029/1999JA900141.
- Ashour-Abdalla, M., M. El-Alaoui, V. Peromian, R. J. Walker, L. M. Zelenyi, L. A. Frank, and W. R. Paterson (1999), Localized reconnection and substorm onset on December 22, 1996, *Geophys. Res. Lett.*, **26**, 3545–3548.
- Ashour-Abdalla, M., M. El-Alaoui, V. Peromian, R. J. Walker, J. Raeder, L. A. Frank, and W. R. Paterson (2000), The origin of the near-Earth plasma population during a substorm on November 24, 1996, *J. Geophys. Res.*, **105**, 2589–2605.
- Ashour-Abdalla, M., M. El-Alaoui, F. V. Coroniti, R. J. Walker, and V. Peromian (2002), A new convection state at substorm onset: Results from an MHD study, *Geophys. Res. Lett.*, **29**, 1965, doi:10.1029/2002GL015787.
- Birn, J., J. C. Dorelli, M. Hesse, and K. Schindler (2004), Thin current sheets and loss of equilibrium: Three-dimensional theory and simulations, *J. Geophys. Res.*, **109**, A02215, doi:10.1029/2003JA010275.
- Birn, J., R. Nakamura, E. V. Panov, and M. Hesse (2011), Bursty bulk flows and dipolarization in MHD simulations of magnetotail reconnection, *J. Geophys. Res.*, **116**, A01210, doi:10.1029/2010JA016083.
- Biskamp, D. (1993), *Nonlinear Magnetohydrodynamics*, Cambridge Monographs on Plasma Physics, Cambridge Univ. Press, Cambridge, U. K.
- Borovsky, J. E., and H. O. Funsten (2003), The MHD turbulence in the Earth's plasma sheet: Dynamics, dissipation, and driving, *J. Geophys. Res.*, **108**(A7), 1284, doi:10.1029/2002JA009625.
- Borovsky, J. E., R. C. Elphic, H. O. Funsten, and M. F. Thomsen (1997), The Earth's plasma sheet as a laboratory for turbulence in high-beta MHD, *J. Plasma Physics*, **57**, 1–34.
- Bruno, R., and V. Carbone (2005), The solar wind as a turbulence laboratory, *Living Rev. Solar Phys.*, **2**, 4, <http://www.livingreviews.org/lrsp-2005-4>.
- Castaing, B., Y. Gagne, and E. J. Hopfinger (1990), Velocity probability distribution functions of high Reynolds number turbulence, *Physica D*, **46**, 177–200.
- Chang, T. (1999), The role of coarse grained helicity and self organized criticality in magnetotail dynamics, in *Magnetic Helicity in Space and Laboratory Plasmas*, edited by M. Brown, R. Canfield, and A. Pevtsov, pp. 277, AGU, Washington, D. C.
- El-Alaoui, M. (2001), Current disruption during November 24, 1996, substorm, *J. Geophys. Res.*, **106**(A4), 6229–6245.
- El-Alaoui, M., R. L. Richard, M. Ashour-Abdalla, and M. W. Chen (2004), Low Mach number bow shock locations during a magnetic cloud event: Observations and magnetohydrodynamic simulations, *Geophys. Res. Lett.*, **31**, L03813, doi:10.1029/2003GL018788.
- El-Alaoui, M., M. Ashour-Abdalla, J. M. Bosqued, and R. L. Richard (2008), Understanding Magnetotail Current Sheet Meso-Scale Structures Using MHD Simulations, *J. Adv. Space Res.*, doi:10.1016/j.asr.2007.05.061.
- El-Alaoui, M., M. Ashour-Abdalla, R. J. Walker, V. Peromian, R. L. Richard, V. Angelopoulos, and A. Runov (2009), Substorm evolution as revealed by THEMIS satellites and a global MHD simulation, *J. Geophys. Res.*, **114**, A08221, doi:10.1029/2009JA014133.
- El-Alaoui, M., M. Ashour-Abdalla, R. L. Richard, M. L. Goldstein, and J. M. Weygand, and R. J. Walker (2010), Global magnetohydrodynamic simulation of reconnection and turbulence in the plasma sheet, *J. Geophys. Res.*, **115**, A12236, doi:10.1029/2010JA015653.
- El-Alaoui, M., R. L. Richard, M. Ashour-Abdalla, M. L. Goldstein, and R. J. Walker (2011), Magnetohydrodynamic turbulence and reconnection in the magnetotail, Abstract SM53A-06, presented at 2011 Fall Meeting, AGU, San Francisco, Calif., 4–9 Dec.
- El-Alaoui, M., R. L. Richard, M. Ashour-Abdalla, R. J. Walker, and M. L. Goldstein (2012), Turbulence in a global magnetohydrodynamic simulation of the Earth's magnetosphere during northward and southward interplanetary magnetic field, *Nonlin. Processes Geophys.*, **19**, 165–175, www.nonlin-processes-geophys.net/19/165/2012/doi:10.5194/npg-19-165-2012.
- Frank, L. A., et al. (1995), Observations of plasmas and magnetic fields in Earth's distant magnetotail: Comparison with a global MHD model, *J. Geophys. Res.*, **100**(A10), 19,177–19,190, doi:10.1029/95JA00571.
- Greco, A., W. H. Matthaeus, R. D'Amicis, S. Servidio, and P. Dmitruk (2012), Evidence for nonlinear development of magnetohydrodynamic scale intermittency in the inner heliosphere, *Astrophys. J.*, **749**(2), 105, doi:10.1088/0004-637X/749/2/105.
- Keiling, A., et al. (2009), Substorm current wedge driven by plasma flow vortices: THEMIS observations, *J. Geophys. Res.*, **114**, A00C22, doi:10.1029/2009JA014114.
- Kolmogorov, A. N. (1941), The local structure of turbulence in incompressible viscous fluid for very large Reynolds numbers, *C. R. Acad. Sci. URSS*, **30**, 301.
- Kraichnan, R. H. (1965), Inertial range of hydromagnetic turbulence, *Phys. Fluids*, **8**, 1385–1387.
- Lui, A. T. Y. (2001), Multifractal and intermittent nature of substorm associated magnetic turbulence in the magnetotail, *J. Atmos. Sol. Terr. Phys.*, **63**, 1379–1385.
- Lyons, L. R., Y. Nishimura, X. Xing, A. Runov, V. Angelopoulos, E. Donovan, and T. Kikuchi (2012), Coupling of dipolarization front flow bursts to substorm expansion phase phenomena within the magnetosphere and ionosphere, *J. Geophys. Res.*, **117**, A02212, doi:10.1029/2011JA017265.
- Montgomery, D. (1987), Remarks on the MHD problem of generic magnetospheres and magnetotails, in *Magnetotail Physics*, edited by A. T. Y. Lui, pp. 203–204, Johns Hopkins University Press, Baltimore, Md.
- Ohtani, S., Y. Miyashita, H. Singer, and T. Mukai (2009), Tailward flows with positive B_z in the near-Earth plasma sheet, *J. Geophys. Res.*, **114**, A06218, doi:10.1029/2009JA014159.
- Oka, M., T.-D. Phan, J. P. Eastwood, V. Angelopoulos, N. A. Murphy, M. Øieroset, Y. Miyashita, M. Fujimoto, J. McFadden, and D. Larson (2011), Magnetic reconnection X-line retreat associated with dipolarization of the Earth's magnetosphere, *Geophys. Res. Lett.*, **38**, L20105, doi:10.1029/2011GL049350.
- Osman, K. T., W. H. Matthaeus, M. Wan, and A. F. Rappazzo (2012), Intermittency and local heating in the solar wind, *Phys. Rev. Lett.*, **108**(2), 261102, doi:10.1103/PhysRevLett.108.261102.
- Peromian, V., M. El-Alaoui, M. A. Abdalla, and L. M. Zelenyi (2006), Dynamics of ionospheric O^+ ions in the magnetosphere during the 24–25 September 1998 magnetic storm, *J. Geophys. Res.*, **111**, A12203, doi:10.1029/2006JA011790.
- Raeder, J., R. J. Walker, and M. Ashour-Abdalla (1995), The structure of the distant geomagnetic tail during long periods of northward IMF, *Geophys. Res. Lett.*, **22**, 349.
- Raeder, J., J. Berchem, and M. Ashour-Abdalla (1996), The importance of small scale processes in global MHD simulations: Some numerical experiments, in *Physics of Space Plasmas*, vol. 14, edited by T. Chang and J. R. Jasperse, pp. 403, MIT Center for Theoretical Geo/Cosmo Plasma Physics, MIT, Cambridge, Mass.
- Raeder, J., J. Berchem, and M. Ashour-Abdalla (1998), The Geospace Environment Modeling Grand Challenge: Results from a Global Geospace Circulation Model, *J. Geophys. Res.*, **103**(A7), 14,787–14,797, doi:10.1029/98JA00014.
- Raeder, J., R. L. McPherron, L. A. Frank, S. Kokubun, G. Lu, T. Mukai, W. R. Paterson, J. B. Sigwarth, H. J. Singer and J. A. Slavin (2001), Global simulation of the Geospace Environment Modeling substorm challenge event, *J. Geophys. Res.*, **106**(A1), 381–395, doi:10.1029/2000JA000605.
- Sergeev, V. A., V. Angelopoulos, D. G. Mitchell, and C. T. Russell (1995), In situ observations of magnetotail reconnection prior to the onset of a small substorm, *J. Geophys. Res.*, **100**(A10), 19,121–19,133.
- Sergeev, V. A., V. Angelopoulos, C. A. Cattell, and C. T. Russell (1996), Detection of localized plasma bubbles in the plasma sheet, *J. Geophys. Res.*, **101**, 10,817–10,826.
- Sorriso-Valvo, L., V. Carbone, P. Veltri, G. Consolini, and R. Bruno (1999), Intermittency in the solar wind turbulence through probability distribution functions of fluctuations, *Geophys. Res. Lett.*, **26**, 1801–1804.
- Vörös, Z., et al. (2004), Magnetic turbulence in the plasma sheet, *J. Geophys. Res.*, **109**, A11215, doi:10.1029/2004JA010404.
- Walker, R. J., M. Ashour-Abdalla, M. El Alaoui, and F. V. Coroniti (2006), Magnetospheric convection during prolonged intervals with southward interplanetary magnetic field, *J. Geophys. Res.*, **111**, A10219, doi:10.1029/2005JA011541.
- Wan, M., W. H. Matthaeus, H. Karimabadi, V. Roytershteyn, M. Shay, P. Wu, W. Daughton, B. Loring, and S. C. Chapman (2012), Intermittent dissipation at kinetic scales in collisionless plasma turbulence, *Phys. Rev. Lett.*, **109**(1), 195001, doi:10.1103/PhysRevLett.109.195001.
- Weygand, J. M., et al. (2005), Plasma sheet turbulence observed by Cluster II, *J. Geophys. Res.*, **110**, A01205, doi:10.1029/2004JA010581.
- Weygand, J. M., M. G. Kivelson, K. K. Khurana, H. K. Swarzl, R. J. Walker, A. Balogh, L. M. Kistler, and M. L. Goldstein (2006), Non self-similar scaling of plasma sheet and solar wind probability distribution functions of magnetic field fluctuations, *J. Geophys. Res.*, **111**, A11221, doi:10.1029/2006JA011808.

- Weygand, J. M., W. H. Matthaeus, S. Dasso, M. G. Kielson, and R. J. Walker (2007), Taylor scale and effective magnetic Reynolds number determination from plasma sheet and solar wind magnetic field measurements, *J. Geophys. Res.*, *112*, A10201, doi:10.1029/2007JA012486.
- Yermolaev, Y. I., V. A. Sergeev, L. M. Zelenyi, A. A. Petrukovich, J.-A. Sauvaud, T. Mukai, and S. Kokubun (1999), Two spacecraft observation of plasma sheet convection jets during continuous external driving, *Geophys. Res. Lett.*, *26*, 177–180.